Transition from a paramagnetic metallic to a cluster glass metallic state in electron-doped perovskite manganites

A. Maignan,* C. Martin, F. Damay, and B. Raveau

Laboratoire CRISMAT, UMR 6508 associée au CNRS, ISMRA et Université de Caen 6, Boulevard du Maréchal Juin, 14050 Caen Cedex, France

J. Hejtmanek

Institute of Physics, Cukrovarnicka 10, 16200 Prague 6, Czech Republic

The study of Mn(IV)-rich manganites $Ca_{1-x}Sm_xMnO_3$ with low electron content corresponding to $0 \leq x \leq 0.12$ demonstrates the large difference of their electronic and magnetic properties with that of Mn(III)-rich manganites. In particular, a metalliclike temperature dependence of the resistivity (ρ) is observed above T_C, the smallest room-temperature $\rho = 10^{-3}$ Ω cm being reached for $x=0.12$. However increasing hopping energy with x suggests the creation of small polarons as e_g electrons are injected into the Mn(IV) matrix. The thermopower (S) measurements confirm the increase of carriers with x and can be described within a single-band metal model. The $\rho(T)$ and $S(T)$ curves exhibit also a transition at a fixed temperature $T_p \sim 110$ K for $0.075 \leq x \leq 0.12$. T_p is related to the appearance of a ferromagnetic component as shown from T-dependent magnetization. Nevertheless, the ac-χ measurements reveal a complex behavior. $CaMnO_3$ exhibits a weak ferromagnetic component ($T_C = 122$ K) whereas for $Ca_{1-x}Sm_xMnO_3$ ($0 < x \leq 0.12$) the $\chi'(T)$ curves are characterized by large bumps at T_m with $T_m < T_C$. Moreover, the shapes of the latter are found to be h_{ac} dependent and T_m is also frequency dependent as shown from $\chi''(T)$ curves. The magnetization measurements indicate a cluster glass state below T_C and demonstrate the lack of long-range ferromagnetism in these electron-doped manganites. [S0163-1829(98)03529-2]

INTRODUCTION

The hole-doped manganites $L_{1-x}A_xMnO_3$, where L is a lanthanide and A is an alkaline earth, corresponding to x smaller than 1/2, have been the purpose of numerous investigations these last years owing to their colossal magnetoresistance (CMR) properties (see, for a review, Refs. 1 and 2). Their behavior has been interpreted on the basis of the double-exchange theory,[3,4] and of dynamic Jahn-Teller effect,[5] so that polarons are now widely invoked to explain the magnetoresistive properties of these oxides.[6]

In contrast to the hole-doped phases, the electron-doped manganites which correspond to Mn(IV)-rich contents have not been extensively studied. This lack of interest can be explained by the fact that manganites such as $Bi_{0.25}Ca_{0.75}MnO_3$ or $L_{0.25}Ca_{0.75}MnO_3$ are characterized by charge ordering phenomena[7–9] and do not exhibit magnetoresistive effects. The recent discovery of new ferromagnetic metallic manganites, $Ca_{1-x}L_xMnO_3$ and $Ca_{1-x}Bi_xMnO_3$, for $x \sim 0.10$,[10,11] has stirred up interest for these compounds since it suggests the possibility of magnetoresistance effects for electron-doped systems. $Ca_{0.9}Bi_{0.1}MnO_3$ and $Ca_{0.9}Eu_{0.1}MnO_3$ exhibit indeed negative magnetoresistance but with a much smaller magnitude than that of Mn(III)-rich manganites.

The existence of ferromagnetism for both Mn(IV) and Mn(III)-rich systems has motivated new investigations of the magnetoresistive properties of the electron-doped manganites. The recent exploration of the series $Ca_{1-x}L_xMnO_3$, varying x by a 0.01 step in the range $0 \leq x \leq 0.20$, has shown

the existence of colossal magnetoresistance for an optimal x value ($x_{opt} \sim 0.135 - 0.16$ depending on L), with resistance ratios reaching several orders of magnitude in a magnetic field of 7 T.[12,13] Such a behavior is, at first sight, similar to that observed in hole-doped manganites $L_{1-x}Ca_xMnO_3$ for $x \sim 0.30$.[14] However, for lower x values, the two systems behave differently. For instance the electron-doped manganites $Ca_{1-x}Sm_xMnO_3$ exhibit a semimetallic behavior in the temperature range 200–300 K for $0 < x \leq 0.12$, whereas the hole-doped manganites $L_{1-x}Ca_xMnO_3$ exhibit insulating properties for similar x values, whatever the temperature.

In order to understand the unexpected behavior of the electron-doped manganites, we have undertaken a detailed study of the oxides $Ca_{1-x}Sm_xMnO_3$, for low electronic density, i.e., in the ferromagnetic region, before the appearance of the CMR effect ($0 < x \leq 0.12$). In the present paper we discuss the transport properties in the paramagnetic state in dependence of x and we see a complex transition at $T \sim 110$ K independent of x below which the samples behave as cluster glasses.

EXPERIMENTAL

The synthesis of the $Ca_{1-x}Sm_xMnO_3$ ($0 \leq x \leq 0.20$) samples was described elsewhere.[12] Purity, cationic homogeneities, and compositions were systematically checked by electron diffraction coupled with EDS analysis and by x-ray diffraction. The ''O_3'' oxygen stoichiometry was determined by iodometric titration for all the series whereas thermogravimetric analysis was also performed at 1000 °C in an Ar/H_2 flow for $CaMnO_3$ ($x=0.00$). With the accuracy of
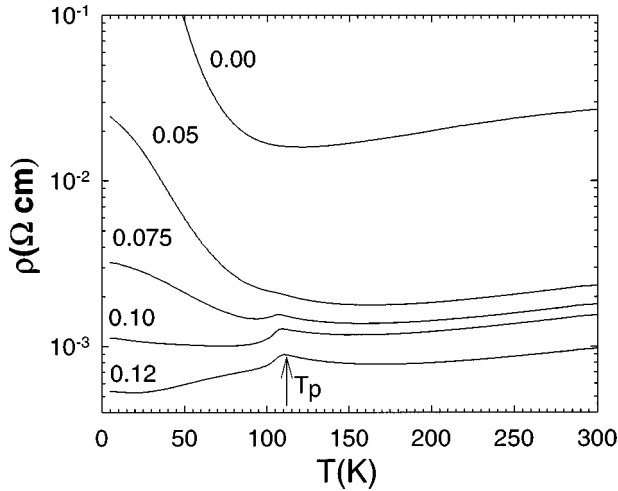
FIG. 1. T-dependent resistivity for the $Ca_{1-x}Sm_xMnO_3$ samples; x values are labeled on the graph. The transition temperature T_p is also shown.

both techniques, the oxygen stoichiometry is found to be equal to 3.00 ± 0.02.

Resistivity measurements were performed with the four-probe method on bars of dimensions $2 \times 2 \times 10$ mm^3 with a Quantum Design physical properties measurement system allowing us to apply magnetic fields in the range 0–7 T and in a temperature range of 5–400 K.

The thermoelectric power (S) measurements were carried out between 11–310 K using close-cycle refrigerator. The four-point steady-state method with separated measuring and power contacts was used to eliminate their thermal resistances. The rectangular-shaped samples were mounted on the heat sink of cryostate and the miniature resistor, attached by a pair of 0.072 mm chromel wires, using GE varnish on the end of the sample as the heater. The temperature gradient and voltage drop was monitored using two differential chromel-constantan thermocouples (0.072 mm in diameter) which were affixed to the sample extremities using copper link, indium solder, and silver paint. A typical temperature difference across the sample was 1.5 K. The influence of the thermopower of chromel was carefully taken into account and necessary correction was made. The experimental setup was checked on high-temperature superconductor Bi-2223 ceramics ($T_c = 108$ K) and chromel wire and the error within all range of temperatures did not exceed 1 μV K^{-1}.

Magnetization data were collected with a Quantum Design superconducting quantum interference device (SQUID) magnetometer (5–400 K, 0–5 T) and with a vibrating-sample magnetometer (5–300 K, 0–1.45 T). ac-χ curves were registered with an ACS 7000 Lake Shore susceptometer (10 Oe; $f = 8, 33, 133$ Hz) or with an ac-dc SQUID magnetometer from Quantum Design (10^{-3} Oe $< h_{ac} \lesssim 3$ Oe; 1 Hz $\leqslant f \leqslant 1$ kHz). Temperature-dependent inverse of the susceptibility curves were obtained from a Faraday balance operating in 0.3 T in the temperature range 100–800 K.

RESULTS AND DISCUSSION

The inspection of the resistivity (ρ) versus temperature curves of $Ca_{1-x}Sm_xMnO_3$ samples (Fig. 1) clearly shows

that the doping of the calcium site with samarium decreases significantly the resistivity with respect to $CaMnO_3$ ($x = 0.00$). The first important point deals with the existence of a semimetallic domain in the range 175–300 K, whatever the x ranging from 0 to 0.12. This behavior, very different from that of the hole-doped manganites $L_{1-x}Ca_xMnO_3$, which are insulating for similar x values, can be explained by the fact that on the Mn(IV)-rich side, the Jahn-Teller effect is weak and consequently the distortion of the $[MnO_3]_\infty$ framework is small, favoring only the weak electron-phonon coupling, contrary to the Mn(III)-rich compositions.

The transport properties of $Ca_{1-x}Sm_xMnO_3$ in the para-magnetic state can be understood supposing the existence of a narrow band with mainly an e_g character which is gradually filled with electrons as calcium is replaced by samarium.[15] With respect to the fact that the e_g band is very narrow the density of states at E_F is supposed to be relatively high; energy fluctuations due to randomness introduced by the chemical substitution, which is necessary to create the charge carriers, can easily induce the carrier delocalization. This should be the case when the concentration of electrons is low and E_F does not reach the mobility edge E_C.[16] When the electrons concentration is increased the usual band mechanism will dominate. Note, however, that due to the mechanism of carrier creation (nonisovalent cationic substitution) and considering the previously mentioned Jahn-Teller effect—the distortion of MnO_6 octahedra due to $t_{2g}^3 e_g^1$ configuration—one can expect a continuous formation of small polarons with increasing x.

The electrical conductivity, expressed by a classical formula

$$\sigma(E) = n(E) * e * \mu(E),$$

is then a compromise between the high carrier mobility $\mu(E)$ (highest for pure $CaMnO_3$ with no disorder and without MnO_6 distortion) and the carrier density $n(E)$ (induced via the Ca/Sm substitution and/or the oxygen vacancies). The carrier creation is, however, unavoidably accompanied by increasing disorder and, as we have mentioned above, by a tendency to form ''polarons'' which move by hopping. In a frame of this picture we have fitted the resistivity data between 200 and 300 K using the formula including both the carrier hopping and their scattering:

$$\rho = A * T * \exp(W/kT),$$

where A is a constant and $W = E_H - J$ represents the hopping energy. The temperature-dependent drift mobility is $\mu_D \sim T^{-1} \exp[-(E_H - J)/kT]$ where E_H is the hopping energy and J is the transfer integral. The observed activation energies W are listed in Table I. Despite the fact that the electrical resistivity dramatically decreases with increasing x, the increase of the activation energies from the very small value ~ 5 meV for $CaMnO_3$ up to ~ 10 meV for sample $x = 0.12$ reflects, according to our opinion, the increasing tendency to form small polarons when the concentration of formally Mn(III) ions increases. Finally let us emphasize that the metallicity observed for $x = 0$ suggests that the carriers result from an oxygen deficiency according to the formulation $CaMnO_{3-\varepsilon}$ with $\varepsilon \leqslant 0.02$.

TABLE I. Transport characteristics for the $Ca_{1-x}Sm_xMnO_3$ series deduced from the resistivity and thermoelectric power measurements and chemical composition. The n_{Mn}/n ratio is calculated according to the chemical composition.

x	$\rho_{(300\,K)}$ (mΩ cm)	W_H (meV)	$S_{(300\,K)}$ (μV K^{-1})	$N(E)/n$	$n_{(Mn)}/n$
0	26.9	5.4	-350	22	
0.05	2.33	8.1	-120	12	20
0.10	1.5	8.4	-65	10	10
0.12	1.0	10.3	-65	7	8

The second point concerns the fact that the resistivity goes through a broad minimum around 160 K and increases again as T decreases below this temperature, whatever x, leading to a semiconductinglike behavior. But most important is the appearance of a peak on the $\rho(T)$ curves as soon as the electron density is sufficient, i.e., for $x>0.05$. Moreover it is remarkable that the peak temperature T_p does not vary with the composition, i.e., $T_p=110$ K whatever x.

The $M(T)$ curves registered under 1.45 T already established for these compounds[12] show that all of them exhibit a ferromagnetic component with $T_C\sim T_p$ (Fig. 2), whose magnitude increases with x so that the magnetic moment reaches its maximum value, 1.1 μ_B, for $x=0.12$. The existence of this peak is likely related to the critical scattering when approaching to the magnetic transition. Note that the weak ferromagnetism observed for $CaMnO_3$ ($x=0.00$) is in agreement with the magnetization measurements performed by different groups.[17–19] The existence of this small ferromagnetic component may be explained by a deviation from the stoichiometric ''O_3'' content that would imply small amounts of e_g electrons on the Mn^{4+} lattice. The metalliclike behavior observed at this composition between 120 and 300 K (Fig. 1) may be understood if only 1 or 2 % of Mn^{3+} are created by the oxygen deficiency and thus inducing delocalization in the narrow e_g band.

A useful insight to better understand the carrier transport consists of measuring T-dependent thermoelectric power (S) (Fig. 3). A common prominent feature for all samples is the negative value, indicating that we are dealing with electrons,
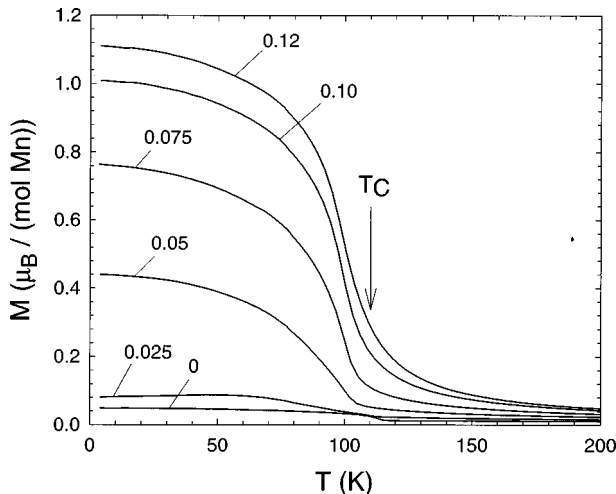
and a linear temperature dependence in the paramagnetic region. The samples exhibit, however, a different behavior in the magnetically ordered state. For the samples with $x\sim0.0$ and 0.05 the thermopower decreases just below T_C, while for the $x=0.10$ sample the thermopower increases. This behavior indicates, independently on the detailed interpretation of the thermopower data, a decrease of the carrier concentration for samples with $x=0.0$ and $x=0.05$ compared to $x=0.10$. For the latter, supposing the metalliclike behavior above T_p and a very slightly increasing resistivity below T_p (Fig. 1) the jump and a change in the thermopower temperature dependence correspond to a change in the transport mechanism; the best fit of both resistivity and thermopower behavior, corresponds to the variable-range hopping in three dimensions.

In order to explain the transport in the paramagnetic region we have used the expression for the thermopower derived from the general formula valid for a single band metal rewritten:

$$S=\pi^2*k_B/3e*k_B*T\{\delta\ln\sigma(E)/\delta E\}_{E=E_f}$$

(δ partial derivative).

Taking into account the above mentioned formula for the electrical conductivity this can be rewritten as

$$S=\pi^2*k_B/3e*k_B*T\{N(E)/n+\delta\ln\mu(E)/\delta E\}_{E=E_f},$$

where $N(E)$ is the density of states and n is the carrier density. When the thermopower is described by this equation, its absolute value increases linearly with temperature and is inversely proportional to the carrier concentration n. This is
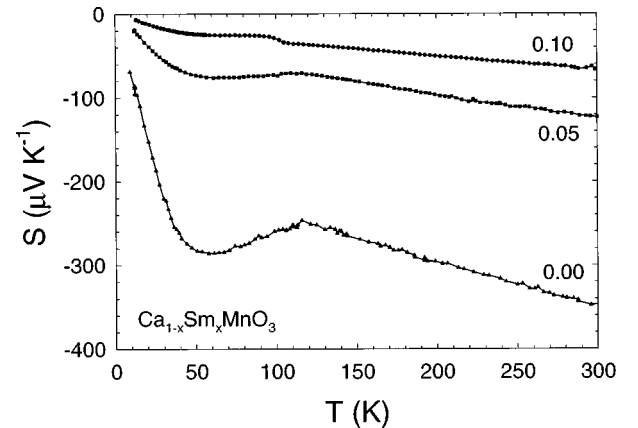

FIG. 2. T-dependent magnetization for the series $Ca_{1-x}Sm_xMnO_3$ ($0\leqslant x\leqslant0.12$) registered during warming in 1.45 T after a zero-field cooling.

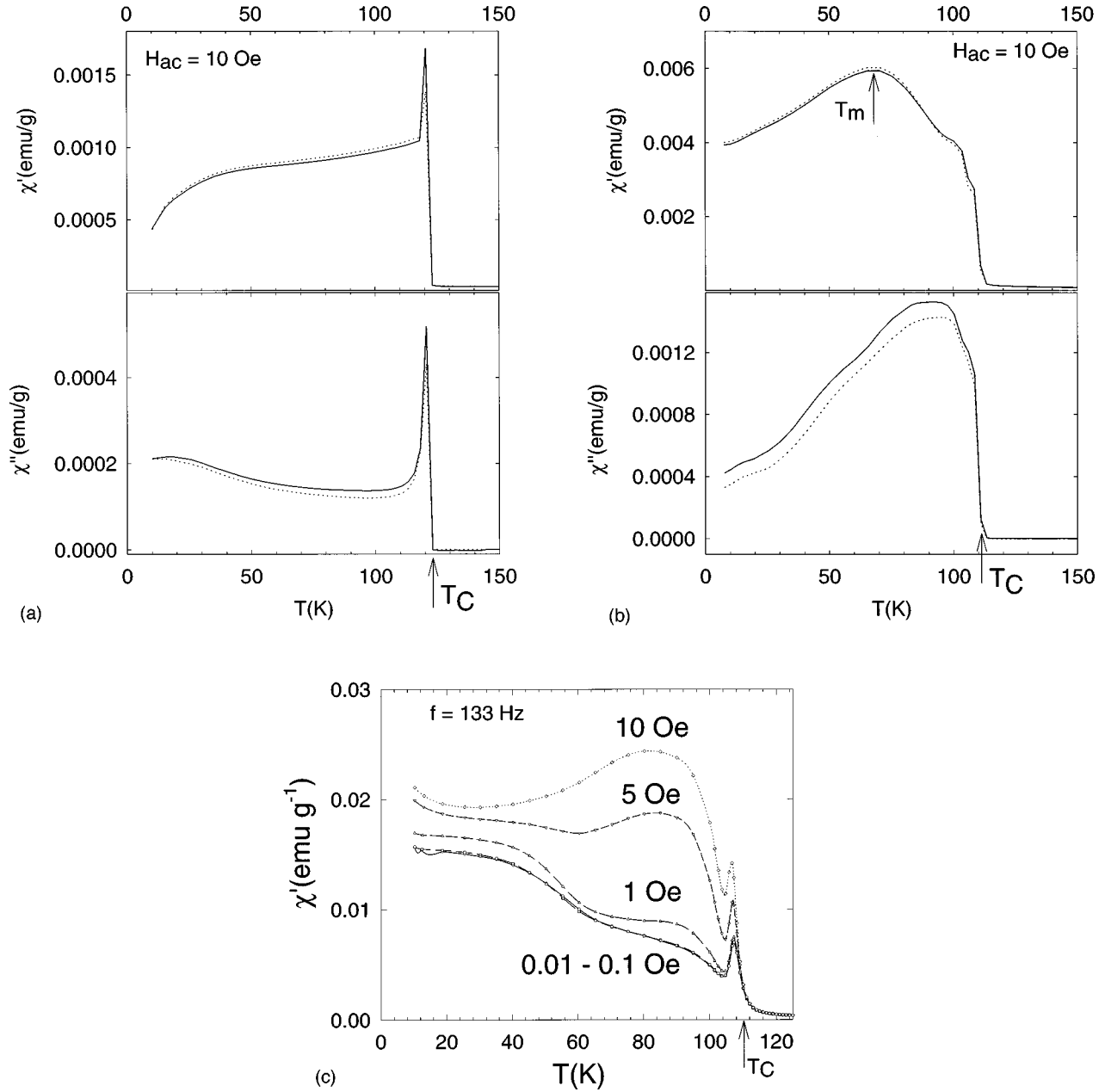FIG. 3. T-dependent thermopower of three $Ca_{1-x}Sm_xMnO_3$ compounds corresponding to the value labeled on the graph.

FIG. 4. (a) T-dependent ac-χ of CaMnO$_3$ [top: real part (χ'), bottom: imaginary part (χ'')]. Solid and dotted lines are for $f = 8$ and 133 Hz, respectively. The arrow on the bottom part indicates the Curie temperature T_C. (b) $\chi'(T)$ (top) and $\chi''(T)$ (bottom) curves of Ca$_{0.975}$Sm$_{0.025}$MnO$_3$. The arrow (top part) indicates the characteristic temperature (T_m) at the bump. (c) $\chi'(T)$ curves for Ca$_{0.90}$Sm$_{0.10}$MnO$_3$ registered at 133 Hz for different h_{ac} excitation fields labeled on the graph. The curves corresponding to $h_{ac} = 10^{-2}$ and 10^{-1} Oe are superimposed.

exactly what is found in our case. By using the experimental conductivity σ and S values, $N(E)/n$ ratios can be calculated (Table I). Using a rough approximation, the $N(E)$ value corresponds to the total concentration of Mn ions $n(\text{Mn}) = 1.8 \times 10^{22}$ cm^{-3} and the Mn(III) concentration is determined by x, $n \sim x*1.8 \times 10^{22}$. One can compare the experimental $N(E)/n$ ratio with the theoretical one, $n(\text{Mn})/n$. This gives surprisingly good agreement between the values of the single-band model used to described the thermopower and chemical composition for the $x = 0.12$ and 0.10 samples. The difference for the $x = 0.05$ and ~ 0.0 samples could be either due to a simplified model or to slight oxygen deficiency for the samples with $x < 0.10$.

The last remarkable feature of the $\rho(T)$ curves concerns the domain below $T_p = 110$ K which corresponds in a first step to a transition toward a second semimetallic state at low temperature. The latter can only be stabilized for a sufficient electron density ($x > 0.10$), whereas for a too low electron density a turn up toward a semiconducting behavior is observed (see for instance $x = 0.075$).

The ac susceptibility (ac-χ) curves (Fig. 4) confirm that the Sm for Ca substitution drastically modifies the magnetic properties. A sharp transition at 122 K on the $\chi'(T)$ curve of CaMnO$_3$ [Fig. 4(a), top] together with nonzero χ'' values [Fig. 4(a), bottom], indicative of weak ferromagnetism with $T_C = 122$ K, is observed. In contrast, the substitution of 2.5%

TABLE II. Characteristic temperatures for the $Ca_{1-x}Sm_xMnO_3$ series deduced from the magnetic measurements: T_C and T_m from the ac-χ curves, θ_p from the $\chi^{-1}(T)$ curves.

x	T_C (K)	T_m (K)	θ_p (K)
0	122		-500
0.025	110	68	-220
0.05	110	70	
0.075	110	69	
0.10	110	84	$+40$
0.12	110	92	

Sm for Ca increases χ' by a factor 4 [Fig. 4(b), top], whereas the Curie temperature (T_C) determined from the $\chi''(T)$ curve [Fig. 4(b), bottom] is decreased to 110 K. Moreover the $\chi'(T)$ curve of this electron-doped phase differs from that of $CaMnO_3$ by the appearance of a broad maximum at $T_m = 68$ K [Fig. 4(b)], which is not expected for a ferromagnet. Similar shapes of the χ' curves are systematically observed, whatever x in the range $0.025 \leq x \leq 0.12$, as illustrated for $x = 0.10$ [Fig. 4(c), upper curve]. It is worth pointing out that the χ' maximum value continuously increases with x, in agreement with the $M(T)$ curves of Fig. 2 whereas the constant value T_C corresponds to T_p on the $\rho(T)$ curves, i.e., $T_C = T_p = 110$ K. Nevertheless, a peak appears at 108 K for $x = 0.075$, which becomes more pronounced as x increases, as shown for $x = 0.10$ [Fig. 4(c)]. Moreover the temperature of the broad maximum T_m tends to increase with x for $x > 0.075$, as shown from the comparison of the T_C and T_m values (Table II).

The existence of ferromagnetic interactions at low temperature is also confirmed by the θ_p increase (Table II). The values are deduced from the extrapolation of the $\chi^{-1}(T)$ curves with 400 K$<T<800$ K. θ_p increases indeed from -220 K for $x = 0.025$ to $+40$ K for $x = 0.10$, so that the $\theta_p < T_C$ relationship is always obeyed confirming the lack of true ferromagnetism. These results show that the ferromagnetism observed at low temperature for these electron-doped manganites, although it corresponds to a metallic state, is very different from the ferromagnetic metallic state previously shown for the hole-doped CMR manganites such as $L_{0.7}Ca_{0.3}MnO_3$.[14]

The curves registered with different ac fields for $Ca_{0.90}Sm_{0.10}MnO_3$ [Fig. 4(c)] clearly show that nonlinear phenomena occur in this compound. It can be seen that $\chi'(T)$ values remain constant for $h_{ac} \leq 10^{-1}$ Oe, whereas the large bump is induced by applying higher h_{ac} values. A nonlinear susceptibility effect is predicted by the mean-field theory for spin glasses with a divergent behavior for the odd harmonics of the susceptibility. Unfortunately with our ac-χ measurement setups, we were not able to separate the different harmonics. One can also remark on this figure that the susceptibility curves start to diverge about 2 K above the peak temperature of 108 K. This characteristic temperature, 110 K, corresponds thus to the Curie temperature in good agreement with the T_C value obtained from the $\chi''(T)$ curve (Fig. 5, bottom). The existence of a nonlinear component has been previously reported for the ''cluster glass'' $La_{0.5}Sr_{0.5}CoO_3$ compound whose clusters originate from lack of long-range ferromagnetic ordering in the vicinity of T_C.[20]
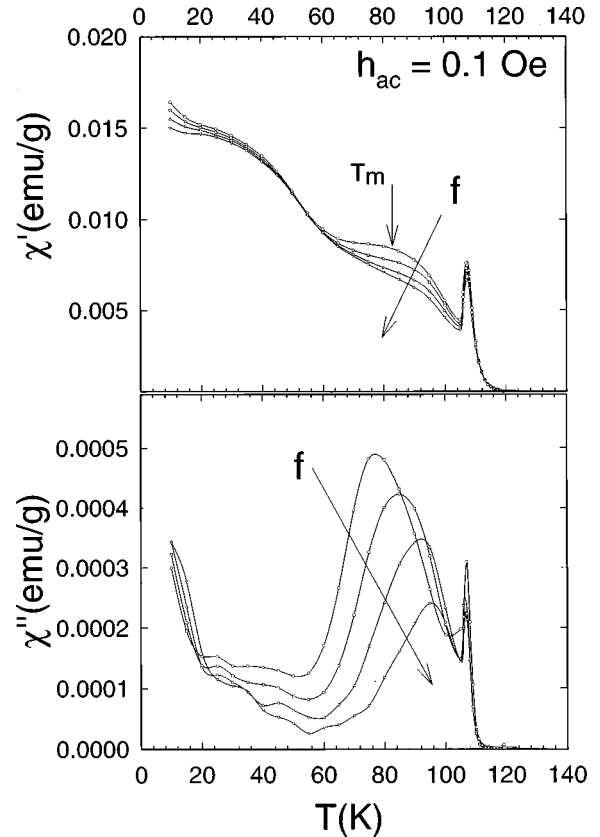

FIG. 5. $\chi'(T)$ (top) and $\chi''(T)$ (bottom) curves of $Ca_{0.90}Sm_{0.10}MnO_3$ registered with $h_{ac} = 0.1$ Oe and four frequencies 1, 10, 100, 1000 Hz increasing in the arrows direction.

In order to test the existence of dynamic effects linked to frozen magnetic domains, the frequency dependence of the ac-χ curves has been checked (Fig. 5). The ac field of 0.1 Oe is in the linear part of the susceptibility. The curves are separated in the bump (T_m) region, clearly demonstrating the existence of dynamic effects below T_C. Moreover, the $\chi''(T)$ maximum (Fig. 5, bottom) is displaced towards high temperatures as f increases, from 68 K to 87 K for $f = 1$ Hz and $f = 1$ kHz, respectively. Such a frequency effect is reminiscent of a spin-glass-like behavior.

Nevertheless the observed behavior for our manganites is a feature encountered in both reentrant spin glasses (RSG) and cluster glass.[20,21] The frequency shift per decade of the temperature T_m on $\chi''(T)$ curves, registered with the low h_{ac} value of 0.1 Oe (linear part), leads to $K = \Delta T_m / T_m \ln \Delta f$ equal to 0.09, which is in agreement with typical values observed for both, cluster and spin glasses.[20–22]

Thus, at this point it is not possible to determine whether these oxides are cluster glasses or reentrant spin glasses, since both exhibit a T_C and a frequency-dependent maximum of $\chi''(T)$. Field-cooled (FC)–zero-field-cooled (ZFC) magnetization measurements allow us to find a clue to this issue. The $M(T)$ curves for $x = 0.10$ (Fig. 6) exhibit a strong hysteresis, in agreement with the lack of a true long-range ordering. Moreover, the irreversibility starts just below T_C, contrary to what appears for RSG, where the FC-ZFC irreversibility occurs significantly below T_C. Furthermore, the field-cooled branch is not flat below the temperature where the FC and ZFC curves start to diverge, contrary to a spin
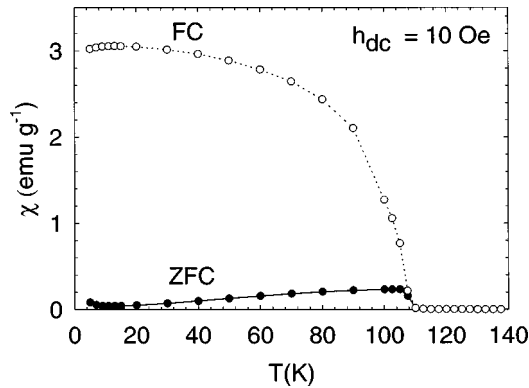
FIG. 6. $\chi(T)$ curves obtained from $M(T)$ curves registered in the ZFC and FC process ($h_{dc} = 10$ Oe) for $Co_{0.9}Sm_{0.1}MnO_3$.

FIG. 7. $M(H)$ curve registered at 10 K for $Co_{0.88}Sm_{0.12}MnO_3$. The arrows indicate the increasing and decreasing branches.

glass, leading to a much larger hysteresis. This demonstrates that $Ca_{0.9}Sm_{0.1}MnO_3$ must be considered as a cluster glass at low temperature.

Finally, according to the similarity of their transport and magnetic behavior, the electron-doped manganites $Ca_{1-x}Sm_xMnO_3$ with $0 < x \leq 0.12$ can be considered as cluster glasses at low temperature in low magnetic field. The application of larger magnetic fields show that the hysteresis curves are not typical of conventional ferromagnets. This is illustrated by the $M(H)$ curve registered for $Ca_{0.88}Sm_{0.12}MnO_3$ at 10 K (Fig. 7). Note, in particular, that the magnetization does not totally saturate and that the remanent magnetization and the coercitive fields remain very small. Furthermore, these $M(H)$ loops together with the $M(T)$ curve (Fig. 2) demonstrate that the saturation magnetization never reaches values close to the expected
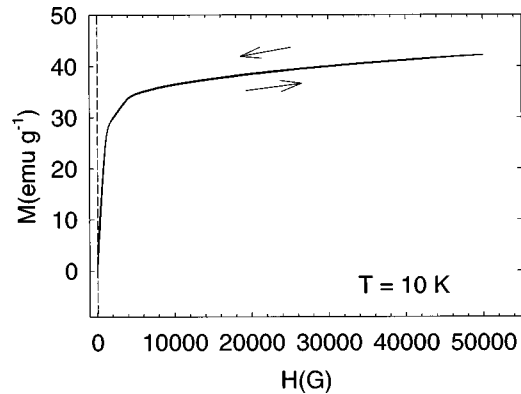
$\sim 3\mu_B$/mole of Mn value but are generally limited to $1 - 1.3\mu_B$ even in magnetic fields of several Tesla.

In conclusion, the combination of transport and magnetic measurements has allowed us to characterize the physical properties of $Ca_{1-x}Sm_xMnO_3$ Mn(IV)-rich manganites ($0 \leq x \leq 0.12$). In particular, a cluster glass magnetic state is observed in low magnetic field below the Curie temperature which is semimetallic for $x = 0.10 - 0.12$, in contrast to the semiconductinglike behavior of Mn(III)-rich manganites. Moreover, the normal-state transport properties always show a semimetallic behavior with a continuous decrease of $\rho_{300\,K}$ from $x = 0.00$ to $x = 0.12$, reaching 10^{-3} Ω cm for the latter. Nevertheless, the fitting of the $\rho(T)$ curves with a small polarons model shows that the hopping energy tends to increase with the doping level. This underlines the crucial role played by the Jahn-Teller Mn(III) e_g^1 cation in the localization process.

*Author to whom correspondence should be sent: Fax: 33 (0)2 31 95 16 00; Electronic address: maignan@crismat.ismra.fr

[1] A. P. Ramirez, J. Phys.: Condens. Matter **9**, 8171 (1997).

[2] B. Raveau, A. Maignan, C. Martin, and M. Hervieu, in *Colossal Magnetoresistance and Related Properties*, edited by C. N. R. Rao and B. Raveau (World Scientific, Singapore, 1998).

[3] C. Zener, Phys. Rev. **82**, 403 (1951).

[4] P. G. de Gennes, Phys. Rev. **118**, 141 (1960).

[5] A. J. Millis, P. B. Littlewood, and B. I. Shraiman, Phys. Rev. Lett. **74**, 5144 (1995).

[6] J. M. de Teresa, M. R. Ibarra, P. A. Algarabel, C. Ritter, C. Marquira, J. Blasco, J. Garcia, A. del Moral, and Z. Arnold, Nature (London) **386**, 256 (1997).

[7] W. Bao, J. D. Axe, C. H. Chen, and S. W. Cheong, Phys. Rev. Lett. **78**, 543 (1997).

[8] Y. Murakami, D. Shindo, H. Chiba, M. Kikuchi, and Y. Syono, Phys. Rev. B **55**, 15 043 (1997).

[9] E. O. Wollan and W. C. Koehler, Phys. Rev. **100**, 545 (1955).

[10] H. Chiba, M. Kikuchi, K. Kusaba, and Y. Syono, Solid State Commun. **99**, 499 (1996).

[11] I. O. Troyanchuk, N. V. Samsonenko, H. Szymczak, and A. Nabialek, J. Solid State Chem. **131**, 144 (1997).

[12] C. Martin, A. Maignan, F. Damay, M. Hervieu, and B. Raveau, J. Solid State Chem. **134**, 198 (1997).

[13] A. Maignan, C. Martin, F. Damay, and B. Raveau, Chem. Mater. (to be published).

[14] A. Maignan, C. Martin, F. Damay, and B. Raveau, Z. Phys. B **104**, 21 (1997).

[15] H. Jung, K. H. Kim, D. J. Eom, T. W. Noh, E. J. Choi, J. Yu, Y. S. Kwon, and Y. Chung, Phys. Rev. B **55**, 15 489 (1997).

[16] N. F. Mott and E. A. Davis, *Electronic Processes in Noncrystalline Materials* (Clarendon, Oxford, UK, 1979).

[17] J. B. Mac Chesney, H. J. William, J. F. Potter, and R. C. Sherwood, Phys. Rev. **164**, 779 (1967).

[18] V. M. Yudin, A. I. Gavrilishina, M. V. Artem'eva, and M. F. Bryzhina, Sov. Phys. Solid State **7**, 1856 (1966).

[19] G. H. Jonker, Physica (Amsterdam) **22**, 707 (1956).

[20] S. Mukherjee, R. Ranganathan, P. S. Anilkumar, and P. A. Joy, Phys. Rev. B **54**, 9267 (1996).

[21] J. E. Greedan, N. P. Raju, A. Maignan, Ch. Simon, J. S. Pedersen, A. M. Niraimathi, E. Gmelin, and M. A. Subramanian, Phys. Rev. B **54**, 7189 (1996).

[22] J. A. Mydosh, *Spin Glasses* (Taylor & Francis, London, 1993).